Philosophical Magazine Letters
Publication details, including instructions for authors and subscription information:
http://www.tandfonline.com/loi/tphl20

Molecular dynamics simulations of the size effect of titanium single-crystal nanopillars orientated for double prismatic slips

Junqiang Ren [a], Qiaoyan Sun [a], Lin Xiao [a], Xiangdong Ding [a] & Jun Sun [a]

[a] State Key Laboratory for Mechanical Behaviour of Materials, Xi'an Jiaotong University, Xi'an, Shaanxi, 710049, P.R. China

Published online: 27 Aug 2013.

To cite this article: Junqiang Ren, Qiaoyan Sun, Lin Xiao, Xiangdong Ding & Jun Sun (2013) Molecular dynamics simulations of the size effect of titanium single-crystal nanopillars orientated for double prismatic slips, Philosophical Magazine Letters, 93:10, 583-590, DOI: 10.1080/09500839.2013.825738

To link to this article: http://dx.doi.org/10.1080/09500839.2013.825738

Philosophical Magazine Letters, 2013
Vol. 93, No. 10, 583–590, http://dx.doi.org/10.1080/09500839.2013.825738

Molecular dynamics simulations of the size effect of titanium single-crystal nanopillars orientated for double prismatic slips

Junqiang Ren, Qiaoyan Sun, Lin Xiao*, Xiangdong Ding and Jun Sun

State Key Laboratory for Mechanical Behaviour of Materials, Xi'an Jiaotong University, Xi'an, Shaanxi 710049, P.R. China

(*Received 7 January 2013; final version received 12 July 2013*)

An inverse "smaller is stronger" trend is predicted on the basis of molecular dynamics simulations of α-titanium (Ti) single-crystal nanopillars orientated for double prismatic slips when the nanopillars are less than 7 nm wide. This trend is attributed to a significant increase in the surface energy due to the nucleation and propagation of edge dislocations on the surface of the pillars.

Keywords: molecular dynamics simulations; titanium single-crystal; dislocations; surface effect

1. Introduction

Titanium (Ti) and its alloys have been widely used in the aerospace and medical industries because of their high specific strength and excellent corrosion resistance. In comparison with the plastic deformation behaviour of highly symmetric cubic metals, that of the anisotropic hexagonal close-packed Ti at the submicron and nanoscales has attracted limited research attention [1,2]. Our previous experiments on the Ti–5Al single-crystal pillars loaded along the $[0\,0\,0\,1]$ direction indicated that the twinning stress increases significantly with decreasing sample size when the external dimensions of the samples are less than 1.0 μm [1]. The plastic deformation was observed through the formation of slips rather than twinning [1]. A microcantilever bend test of the α- and near-α-Ti alloys performed by Gong et al. [2] suggested that an increase in the critical resolved shear stress reduced the cantilever width.

The concept of "smaller is stronger" has been well accepted thus far because a dramatic increase in yield stress was observed in Ni single-crystal pillars under compression loading on the submicron scale [3]. However, as the sample dimensions are further decreased to the nanoscale, the mechanical behaviour of the materials depends on intrinsic (i.e. the initial microstructure and specific size-dependent deformation mechanisms) and extrinsic size effects, such as variations in the sample shape and size, and the contact and loading procedures [4–6]. On the basis of their molecular dynamics (MD) simulations, Rabkin and Srolovitz proposed that yield stress is influenced by the sample shape [6]. The outermost surface layer, especially in the corner of the nanopillars with a square

*Corresponding author. Email: lxiao@mail.xjtu.edu.cn

cross-section, preferentially reaches the critical strain of the dislocation source nucleation; thus, the surface controls the yield stress of the nanopillars.

Because the surface-to-volume ratio of nanoscale materials, including nanowires and nanopillars, is high, the influence of the free surface on plasticity has been the subject of numerous investigations over the last decade [7–11]. Studies on the deformation mechanism of the single-crystal nanopillars via MD simulations suggested that the primary yielding behaviour under uniaxial compression is controlled by the nucleation of a Shockley partial dislocation on the surface [7]. The MD work reported by Afanasyev et al. [8] indicated that dislocations could also nucleate on an interface perpendicular to twins. An asymmetry of the yield stress with a decrease in the width of gold nanowires was observed by Diao et al., who attributed the asymmetry to a surface-stress-induced change in the stable structure [9,12]. Furthermore, Dutta et al. [11] proposed a model involving lattice resistance for the dislocation movement in a nanosized system in which the dislocation velocity increased due to the surface effect.

The Finnis–Sinclair many-body potential is considered more suitable than the embedded atom method [13] and the modified embedded atom method [14] potentials for describing the defect evolution in a single Ti crystal [15] because it accurately describes the physical properties of the Ti according to the calculated energies of the point defects, surfaces, elastic constants and planar faults in the equilibrium structure. An MD simulation with a Finnis–Sinclair type of many-body potential has been successfully employed to describe a variety of defects, surfaces, twin boundaries and atomic interactions within Ti [15–17]. This work aims to predict and analyse the effects of sample size on the mechanical behaviour, dislocation nucleation, movement and interaction in single-crystal Ti during loading and to provide a reasonable explanation of the size effect on the nanoscale based on MD simulations.

2. Simulation method

MD simulations were performed using the large-scale parallel MD program LAMMPS [18] and were visualized using the AtomEye visualization program [19]. The computational supercell had the dimensions $x=[1\,\bar{1}\,0\,0]$, $y=[1\,1\,\bar{2}\,0]$, and $z=[0\,0\,0\,1]$, with a free-surface boundary condition. To investigate the size effect, the sample width was varied from 3 to 15.3 nm. The height-to-width ratio of all of the nanopillars considered for the simulations was 2:1. The single-crystal nanopillars containing 3240–362,850 atoms were compressed along a double prismatic slip orientation of $[1\,1\,\bar{2}\,0]$. The nanopillar length, which could be effectively simulated, ranged from 6.0 to 30.6 nm. A time step of 1.0 fs and a strain rate of $1\times10^{8}\,\mathrm{s}^{-1}$ were chosen. A canonical ensemble – i.e. a constant atom number, volume and temperature – was applied to maintain the system temperature at a constant 300 K. The structure was relaxed using the steepest descent algorithm. The system energy was minimized through iterative adjustments of the coordinates of the atoms.

In MD simulations with the Finnis–Sinclair many-body potential, the basic energy equation of an individual atom can be expressed as

$$E_i = \frac{1}{2}\sum_j V(r_{ij}) - \rho_i^{1/2} \tag{1}$$

where V is the pairwise function between neighbouring atoms i and j.

The potential, ρ_i, is given by

$$\rho_i = \sum_j \phi(r_{ij}) \tag{2}$$

where ϕ is the electronic density function, and r_{ij} is the distance between atom i and one of its neighbouring atoms j.

The pairwise function is

$$V(r) = \sum_{k=1} a_k (r_k - r)^3 H(r_k - r) \tag{3}$$

and the electronic density function can be described as follows:

$$\Phi(r) = \sum_{k=1} A_k (R_k - r)^3 H(R_k - r) \tag{4}$$

where

$$H(x) = \begin{cases} 1, \\ 0, \end{cases} \quad \text{for} \quad \begin{cases} x > 0, \\ x < 0. \end{cases}$$

and A_k, R_k, a_k and r_k are parameters determined by Ackland [15].

3. Results and discussion

A series of MD simulations were performed with various nanopillar widths subjected to uniaxial compression along a $[1\,1\,\bar{2}\,0]$ double prismatic slip orientation at 300 K. The typical stress and strain curves of the nanopillar are provided in Figure 1a and b. Notably, the stress presented in Figure 1 is the average of all atoms in the system. The yield stress, which is the maximum stress sustained by the nanopillar, is 6.94 GPa for a 15.3-nm-wide nanopillar and increases to 8.86 GPa as the width of the nanopillar decreases to 7 nm. A sharp softening stage is displayed after yielding for all of the considered nanopillars (Figure 1). The yield stress as a function of the sample width is described further in Figure 2. An inverse linear relationship is observed between the yield stress and the sample width at widths greater than 7 nm, which indicates that the conventional size effect, i.e. "smaller is stronger", is demonstrated until a critical width of 7 nm (Figures 1a and 2). In comparison, when the nanopillar width is less than 7 nm, the yield stress decreases continuously from 8 GPa in the 6-nm nanopillar to 6.28 GPa in the 3-nm-wide nanopillars (Figure 2), thereby demonstrating an inverse size effect, i.e. a proportional relationship was achieved between the yield stress and the pillar width when the width was less than 7 nm (Figures 1a and 2). A close examination suggested that cyclic hardening was followed by a dramatic softening as the plastic deformation progressed during loading.

Further MD simulations were performed to predict the substructure evolution with the plastic deformation. Figure 3a–d illustrate typical snapshots of the deformed 6-nm-wide

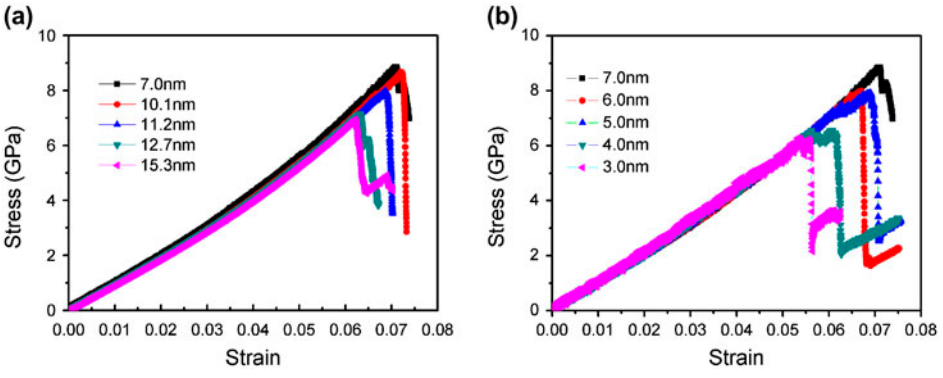

Figure 1. (colour online). Compressive stress–strain curves in nanopillars with various widths: (a) greater than 7 nm and (b) less than 7 nm.

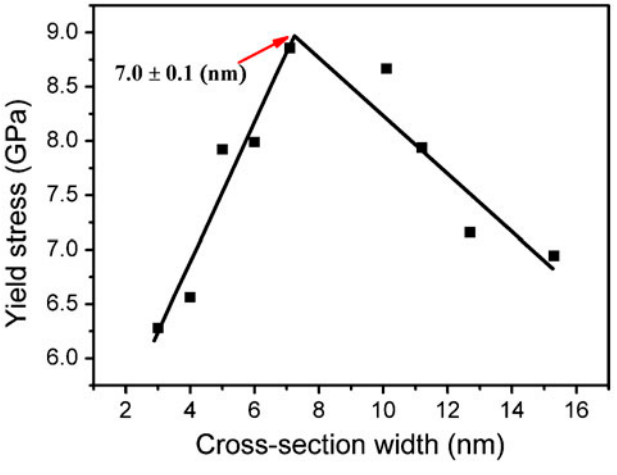

Figure 2. (colour online). The dependence of the yield stress on the pillar width.

pillars along the (0 0 0 1) crystal plane. Each illustration corresponds to the different stages of deformation, as indicated by points A–D in the stress–strain curve in Figure 3e. The surface atoms on the (0 0 0 1) plane and the perfect atoms in the pillar interiors were removed to distinguish the defects. The atoms were coloured according to common-neighbour analysis [20]. The non-coordinated atoms in the vicinity of the vacancies and free surfaces are marked in red (Figure 3). No defects existed in the interior of the initial nanopillar (Figure 3a); however, as the compression stress increased to its maximum value at point B in Figure 3e, the dislocation sources were activated, as shown in Figure 3b, followed by the occurrence of dislocation multiplication in the upper or low corner of the nanopillars, where the stress was concentrated. As the plastic deformation progressed, the dislocation movement was observed, as indicated by the blue arrows in Figure 3b and c. The stress gradually decreased to the local valley at point C, which is attributed to the rapid slip of the dislocations from the interior plane to the nanopillar surfaces, and resulted

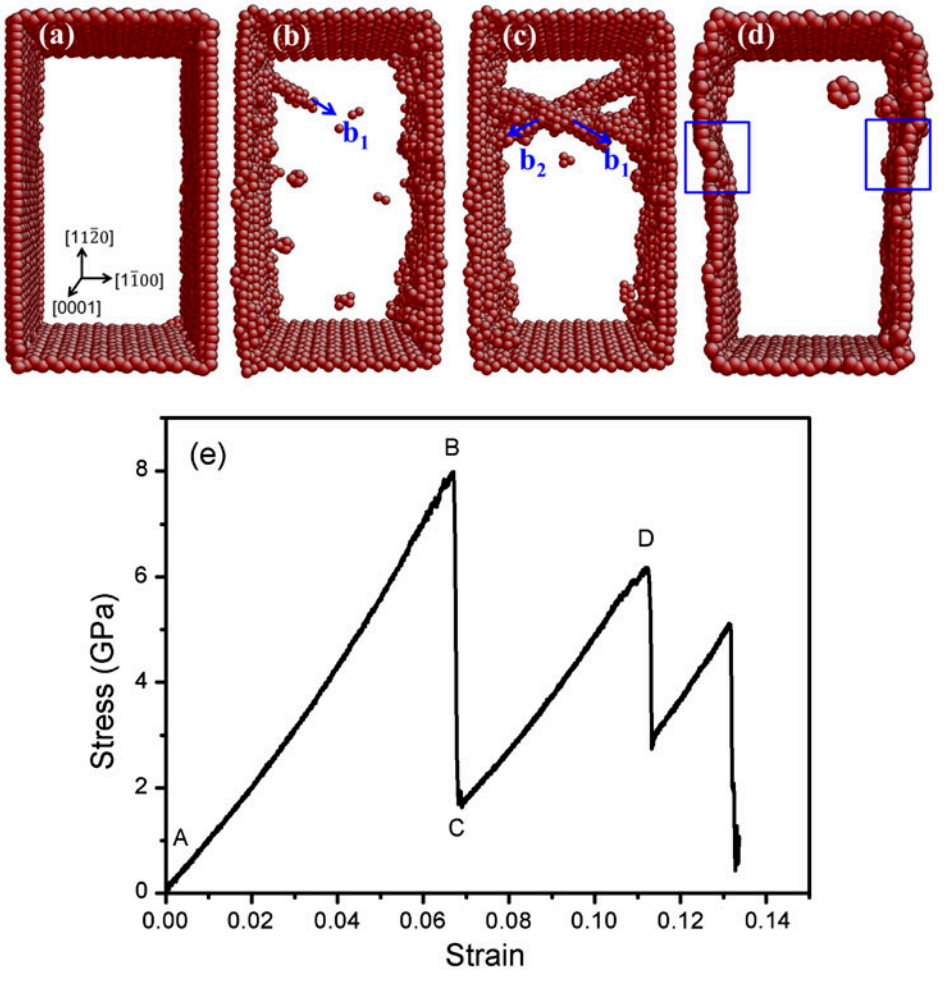

Figure 3. (colour online). Snapshots of a 6-nm-wide $[1\,1\,\bar{2}\,0]$ Ti nanopillar subjected to compressive loading: (a) to (d) correspond to different deformation stages indicated by points A to D in the compressive stress–strain curve shown in (e).

in the accumulation of slip steps on the surface, as indicated by the two blue squares in Figure 3d at point D. The height and density of the surface steps gradually increased as the dislocation continuously escaped from the interior to the surface of the nanopillars. As a result, the dislocation could easily nucleate and grow in the centre of the pillars due to the local stress concentration. Therefore, the stress at point D is lower than that at point B. As the plastic deformation progressed, the stress gradually accumulated to the next yield point. The nucleation and propagation of the new dislocation sources at point D led to a stress fluctuation and effectively released the local stress concentration, thereby causing a decrease in the compression stress. Figure 3b and c are snapshots taken at the points labelled B and C on the curve in Figure 3e. The dislocation clearly nucleated and grew in the corner of the pillar along the $(\bar{1}\,0\,1\,0)$ and $(0\,\bar{1}\,1\,0)$ double prismatic slip planes at a 120° angle as the plastic deformation progressed (Figure 3c). The Burgers vectors were

determined to be $\boldsymbol{b_1} = \boldsymbol{a}/3[1\,\bar{2}\,1\,0]$ and $\boldsymbol{b_2} = \boldsymbol{a}/3[\bar{2}\,1\,1\,0]$ on the basis of the crystallographic analysis and our previous TEM results [21], which indicate that the double prismatic slips $(\bar{1}\,0\,1\,0)$ $[1\,\bar{2}\,1\,0]$ and $(0\,\bar{1}\,1\,0)$ $[\bar{2}\,1\,1\,0]$ were activated under compression along $[1\,1\,\bar{2}\,0]$ (Figure 3b and c). Furthermore, these dislocations were determined to be edge-type because they were perpendicular to the Burgers vectors. These edge dislocation lines were initiated and propagated along the slip plane and finally disappeared from the nanopillar surfaces (Figure 3d).

The potential energy is greatest on the outermost surface atomic layer [4]. The surface-to-volume ratio of the materials rapidly increases when the sample size is less than 10 nm. The surface effect could lead to a large potential energy on several of the outermost surface atomic layers after relaxation, especially in the corners of square nanopillars. Therefore, the surface effect plays an important role in controlling the nucleation and growth of the dislocations in the nanopillars [6,22].

The potential energy of the system was calculated in both a large nanopillar (11 nm in width) and a small nanopillar (4 nm). Figure 4a and b present the potential energy

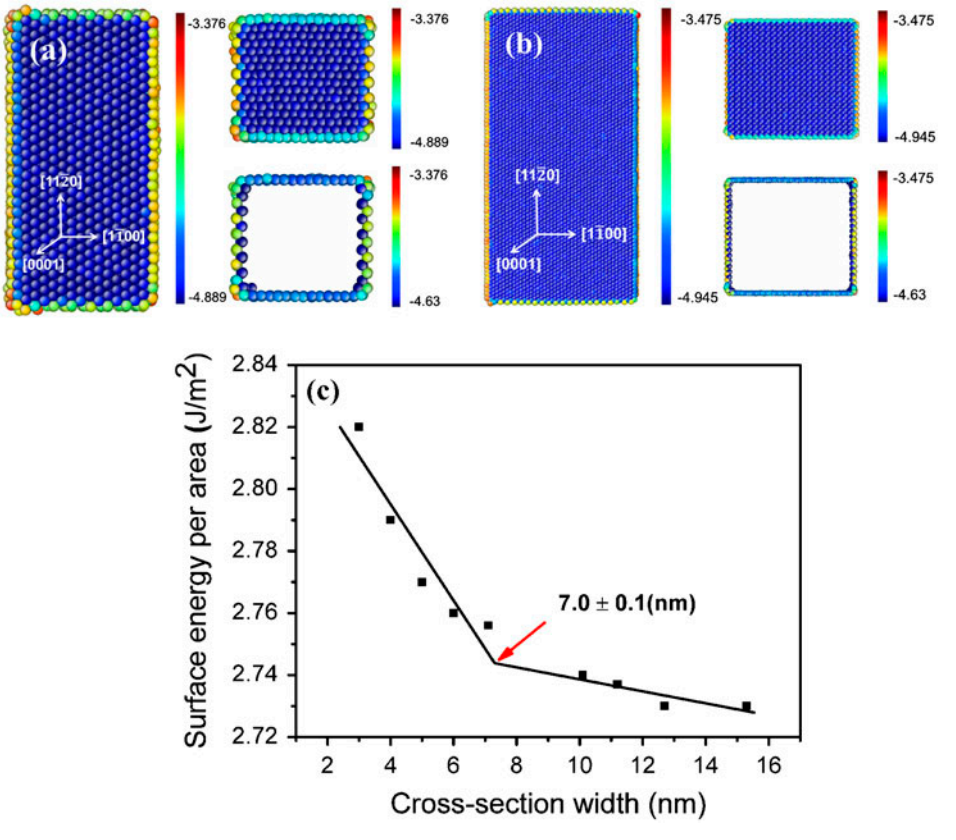

Figure 4. Potential energy distribution of the relaxed square pillar and sectional view along $(0\,0\,0\,1)$ and $(1\,1\,\bar{2}\,0)$ in samples with various widths: (a) 4 nm and (b) 11 nm. (c) The variation in the average surface energy per area with the pillar width.

and the surface atom images on the $(0\,0\,0\,1)$ and $(1\,1\,\bar{2}\,0)$ planes of pillars after relaxation, respectively. The maximum potential energy in the corner of the 4-nm-wide nanopillar was found to be greater (−3.376 eV) than that of the 11-nm nanopillar (−3.475 eV). The potential energy of the atoms on the outermost surface layer increased with decreasing width. Further examination indicated that the potential energy on the two or three outermost surface atomic layers was greater than that on the inside layers due to the surface effect, as shown in Figure 4a and b. The potential energy of the atoms on the $\{1\,\bar{1}\,0\,0\}$ surface exceeds those on the other crystallographic planes. Thus, dislocations easily nucleate on these sites, thereby making surface nucleation a dominant plastic deformation mechanism. Furthermore, the average surface energy per area was calculated as a function of the width of the Ti nanopillars, as shown in Figure 4c. A transition occurs in the surface energy at 7 nm, which is in agreement with the critical nanopillar width for the inverse size effect. In this case, the plastic deformation behaviour of the Ti single crystal is dominated by the dislocation surface nucleation.

Each atom in the interior of a nanopillar is uniformly pulled along different directions by its neighbouring atoms and has a zero net force. However, atoms on the surfaces are pulled inward by the other atoms inside the nanopillars [23,24]. Therefore, the atoms on the surface are subjected to an inward force, which promotes the atomic displacement and local plastic deformation on the surface layers, especially in the corners of the nanopillars. The surface tensile stress increased with the number of surface atoms. Due to the lack of nearest neighbours and weak binding, atoms on the free surfaces and at the corners are typically more active than those in the interior. As a result, the free surfaces and corners become favourable sites for dislocation nucleation.

Rabkin and Srolovitz [6] suggested that the slip would nucleate on the surface when thermal vibrations reached a maximum. The relationship between yield stress and thermal strain can be expressed as:

$$\sigma_y = f(\varepsilon_c - \varepsilon_{therm}) \tag{5}$$

where σ_y is the yield stress, ε_c is the critical atomic strain of slip nucleation and ε_{therm} is the thermal strain. The temperature dependence of the yield stress is determined by the average vibration amplitude of the surface atoms. Furthermore, Cai et al. [25] hypothesized that entropy influences the rate of dislocation nucleation. The large activation entropy on the surface was attributed to the weak atomic bonding caused by thermal expansion and softening, which result in easy nucleation of a dislocation source.

The variation in the surface energy is limited when the width exceeds 7 nm, thereby leading to the conventional size effect. However, the image forces from the free surface promote the disappearance of mobile dislocations in the interiors of large pillars. The dislocation lines nucleated and terminated on the surface. The two ends of the dislocation lines on the surface moved faster than those in the middle. Consequently, the dislocation lines tend to straighten as they glide towards the interior of the pillars and quickly move to the surface when the pillar width exceeds 7 nm. A similar phenomenon has been observed in gold particles [26]. The escape rate of the dislocation lines from the free surfaces exceeds that of the multiplication, which results in the dislocation starvation effect.

4. Conclusions

On the basis of MD simulations, an inverse "smaller is stronger" effect has been predicted in Ti nanopillars with widths less than 7 nm that are orientated for double prism slips. This prediction was attributed to the surface effect caused by a thermal vibration of the surface atoms. The surface becomes the primary dislocation source in the defect-free nanopillars. The plasticity of the pillars is predominantly produced by the edge dislocation lines, which nucleate on the surface when the pillar width is less than 7 nm.

Acknowledgements

This project was supported by the National Natural Science Foundation of China (51271136, 51071118, 51171140 and 50831004) the 973 Programme of China (2010CB631003), and the 111 Project of China (B06025).

References

[1] Q. Yu, Z.W. Shan, J. Li, X.X. Huang, L. Xiao, J. Sun and E. Ma, Nature 463 (2010) p.335.
[2] J.C. Gong and A. Wilkinson, Acta Mater. 59 (2011) p.5970.
[3] M.D. Uchic, D.M. Dimiduk, J.N. Florando and W.D. Nix, Science 305 (2004) p.986.
[4] E. Demir, D. Raabe and F. Roters, Acta Mater. 58 (2010) p.1876.
[5] J.D. Nowak, A.R. Beaber, O. Ugurlu, S.L. Girshick and W.W. Gerberich, Scr. Mater. 62 (2010) p.819.
[6] E. Rabkin and D.J. Srolovitz, Nano Lett. 7 (2007) p.101.
[7] E. Rabkin, H.S. Nam and D.J. Srolovitz, Acta Mater. 55 (2007) p.2085.
[8] K.A. Afanasyev and F. Sansoz, Nano Lett. 7 (2007) p.2056.
[9] J.K. Diao, K. Gall and M.L. Dunn, Nano Lett. 4 (2004) p.1863.
[10] T. Zhu, J. Li, A. Samanta, A. Leach and K. Gall, Phys. Rev. Lett. 100 (2008) p.025502.
[11] A. Dutta, M. Bhattacharya, P. Barat, P. Mukherjee, N. Gayathri and G.C. Das, Phys. Rev. Lett. 101 (2008) p.115506.
[12] J. Diao, K. Gall, M.L. Dunn and J.A. Zimmerman, Acta Mater. 54 (2006) p.643.
[13] R.R. Zope and Y. Mishin, Phys. Rev. B 68 (2003) p.024102.
[14] Y.M. Kim, B.J. Lee and M.I. Baskes, Phys. Rev. B 74 (2006) p.014101.
[15] G.J. Ackland, Philos. Mag. A 66 (1992) p.917.
[16] G.J. Ackland, S.J. Wooding and D.J. Bacon, Philos. Mag. A 71 (1995) p.553.
[17] A. Serra and D.J. Bacon, Acta Mater. 43 (1995) p.4465.
[18] S. Plimpton, J. Comput. Phys. 117 (1995) p.1.
[19] J. Li, Modell. Simul. Mater. Sci. Eng. 11 (2003) p.173.
[20] J.D. Honeycutt and H.C. Andersen, J. Phys. Chem. 91 (1987) p.4950.
[21] Q.Y. Sun, Q. Guo, X. Yao, L. Xiao, J.R. Greer and J. Sun, Scr. Mater. 65 (2011) p.935.
[22] Z.Y. Yang, Z.X. Lu and Y.P. Zhao, J. Appl. Phys. 106 (2009) p.023537.
[23] J.K. Diao, K. Gall and M.L. Dunn, Nat. Mater. 2 (2003) p.656.
[24] M.A. Meyers, A. Mishra and D.J. Benson, Prog. Mater Sci. 51 (2006) p.427.
[25] S. Ryu, K. Kang and W. Cai, Proc. Nat. Acad. Sci. USA 108 (2011) p.5174.
[26] D. Mordehai, S.W. Lee, B. Backes, D.J. Srolovitz, W.D. Nix and E. Rabkin, Acta Mater. 59 (2011) p.5202.